**Supplementary information**

**Methods**

**P-OLC synthesis.** OLC was produced by thermal annealing of ultra-disperse nanodiamond powder purchased from Beijing Grish Hitech Co. at 1100 $^{o}$C for 4 h under protection of argon atmosphere. The as-prepared sample was added to nitric acid with stirring for 4 h at 120 $^{o}$C. The product was then filtered and washed with water and ethanol, and dried at 60 $^{o}$C for 24 h. Two methods were applied to synthesize the phosphorus modified OLC. The first one is the impregnation of OLC with phosphate $(NH_4)_2HPO_4$ and subsequent calcination at 700 $^{o}$C under argon atmosphere. The second one is the CVD method using triphenylphosphine (TPP) as the phosphorous source, which is vaporized to the hot zone of quartz tube by Ar flow, where the OLC are loaded and heated to 600$^{o}$C, 700$^{o}$C, and 800$^{o}$C, respectively.

**Materials characterizations.** High resolution transmission electron microscopy (HRTEM) was performed using a FEI Cs-corrected Titan 80-300 microscope and a FEI Tecnai G2 F20 microscope. XPS was performed with an ESCALAB 250 instrument with an Al $K_{\alpha}$ (1489.6eV). Raman spectra were recorded with a LabRam HR 800 spectrometer with excitation at 532 nm with 25 mW laser power at 2.5 $cm^{-1}$ resolution. Fourier-transform infrared spectroscopy (FT-IR) was performed by using a Nicolet FT-IR infrared microscope with an ATR attachment (ATR-IR).Thermogravimetric (TG) analysis was performed on a NETZSCH STA 449 F3 instrument under a flow of argon or air (50 mL $min^{-1}$) with a heating rate of 10 $^{o}Cmin^{-1}$. Temperature-programmed desorption (TPD) experiments were performed under a He atmosphere. The temperature program involved heating at 10$^{o}$C/min from ambient temperature to 120 $^{o}$C, at which it was kept for 120 min, and then the temperature was raised to 1000$^{o}$C at 5$^{o}$C/min. The product gases were analyzed by online MS (Pfeiffer-Balzer Omnistar). The physical surface area was determined by N2 adsorption/desorption measurements at 77 K by utilizing a Micromeritics ASAP 2020 BET apparatus. Brunauer-Emmett-Teller (BET) formulations were used to calculate the surface area. Pore-size distributions were estimated by applying the

Barrett-Joyner-Halenda (BJH) method to the desorption branch of isotherms.UPS was performed with an ES-CALAB 250 XPS system with a monochromated $AlK_{\alpha}$ X-ray source and a He discharge lamp (He I:*hv* =21.22 eV). The conductivity of the samples is measured with ST2263 four probe tester (Suzhou Jingge Eletronic Co., LTD) at room temperature.

**Electrochemical tests of $CO_2$ reduction.** All the electrochemical measurements were carried out by Electrochemical Station (VMP3, Bio-Logic Science Instruments) at 25 $^{o}$C. A graphite rod was used as counter electrode to avoid any metal contaminant. The working electrode was fabricated by coating 15 μL catalyst ink into 3 mm glassy carbon electrode. The catalyst ink was prepared using 1 mg of the sample carbons dispersed into 1 mL of ethanol containing 50 μL Nafion solution. The Ag/AgCl reference electrode was applied for the potential measurements. The potential was converted to reversible hydrogen electrode potential (RHE) using the *E (vs. RHE) = E (vs. Ag/AgCl) + 0.210 V + 0.0591 × pH (7.5 in 0.5 M $NaHCO_3/CO_2$)*. The $CO_2$ (99.9999%, purity, Dalian Special Gases Co., Ltd) electrochemical reduction tests were conducted in a gas-tight two-compartment electrochemical cell using a piece of Nafion 115 membrane as the separator. Each compartment contained 130 mL electrolyte and 30 mL headspace. Before the $CO_2$ electrochemical reduction, the electrolyte in the cathodic compartment was saturated with $CO_2$ gas for at least 1 h. During the reaction, electrolyte in both compartment was stirred at rate of 800 rpm using a magnetic stirrer.

For the analysis of the gas phase products, an online gas chromatograph (SP-3420A, Beijing Beifen-Ruili Analytical Instrument Group) was used with two Hayesep Q columns, a HP-PLOT/$Al_2O_3$ column (50 m × 0.32 mm × 8μm) and a molecular sieve column. $H_2$, CO, and $CO_2$ were detected with thermal conductivity detector (TCD), and hydrocarbons ($C_xH_y$) were detected with flame ionization detector (FID). The GC was calibrated using calibration curves of analytical gas standards (Dalian Special Gases Co., Ltd).

The Faradaic efficiency (FE) of gas phase product at each applied potential was

calculated based on the following equations:

*FE = (the charge for the generation of product) / (the total consumed charge)*

$= (z * P_0 * F * v * v_j) / (R * T * j)$

*Where:*

*z represented the number of electrons transferred per mole of gas product;*

*$v_j$ was volume concentration of gas product determined from GC;*

*j (A) was steady-state cell current at each applied potential;*

*v ($m^3$ $s^{-1}$ ) was gas flow rate;*

*$P_0 = 1.01 \times 10^5$ Pa;*

*$T_o = 273.15$ K;*

*F = 96500 C $mol^{-1}$;*

*R = 8.314 J • $mol^{-1}$ •$K^{-1}$*

**DFT calculations.** Density functional theory calculations are performed by using Gaussian 09 at B3LYP/6-31G (d,p) level.[1]Three different catalyst models are constructed to represent P-C and P-O bonding configurations respectively as shown in Figure S4. The binding energy is calculated by following equation,

$E_{ads} = E_{adsorbent/slab} - E_{adsorbent} - E_{slab}$

Where $E_{ads}$ is the binding energy, $E_{adsorbent/slab}$ is the total energy of COOH on slabs of catalyst models as shown in Figure 7, $E_{adsorbent}$ is the energy of COOH and $E_{slab}$ is the energy of the catalyst models without adsorption. A negative $E_{ads}$ indicates exothermic process.

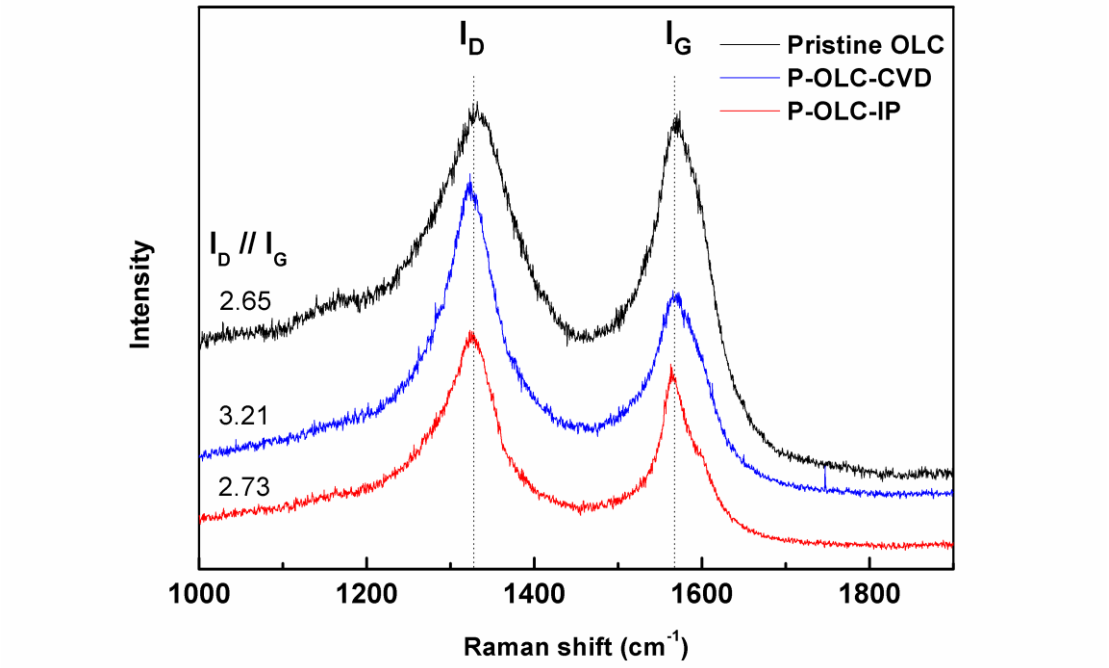


**Figure S1.** Raman spectra of pristine OLC, P-OLC-CVD and P-OLC-IP.

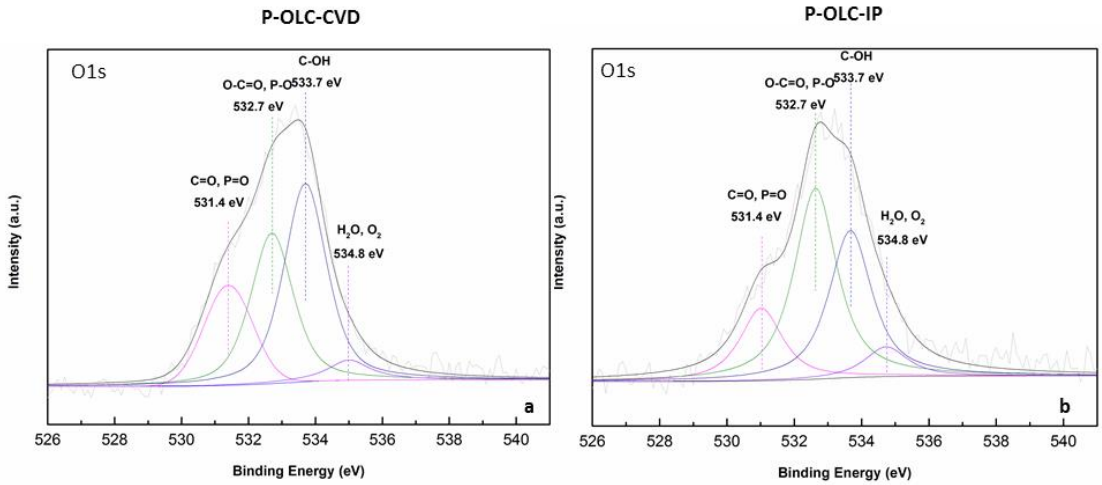


**Figure S2.** (a) O1s XPS spectra of P-OLC-CVD, and (b) P-OLC-IP

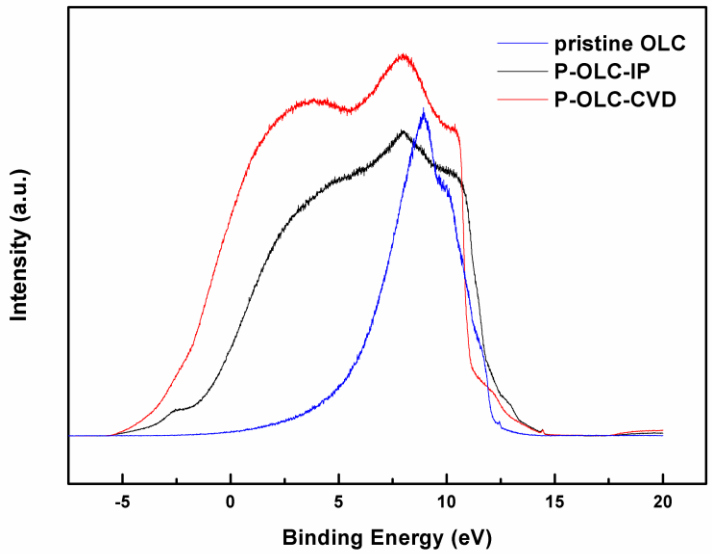


**Figure S3.** UPS spectra of pristine OLC, P-OLC-IP, and P-OLC-CVD samples. UPS spectra are obtained at room temperature using a He discharge lamp (He I: *hv* =21.22 eV). The samples are biased by about -6 V during the work function measurements to accelerate the low energy secondary electrons (SE) and nickel metal is used as reference. The work function ($\Phi$)= 21.22 eV-$|E_{SE} - E_F|$. $E_F$ is the Fermi edge.

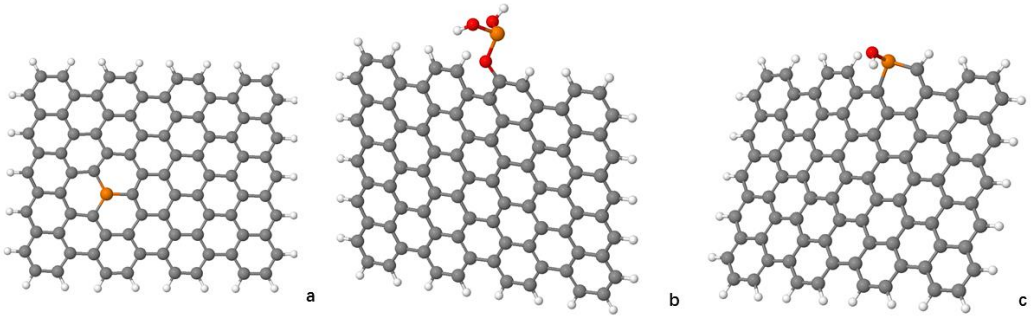


**Figure S4.** The complete structure of phosphorus-doped graphene corresponding to Figure 4 in manuscript, (a) P-C bonding on basal graphitic plane (b) P-O model on the armchair edge (c) P-C bonding on armchair edge..

**Table S1** The FE, major product, onset potential, and current density of CO at highest FE for doped carbon catalysts in CERR.

| Catalyst | FE | Major product | Onset potential | Current density of CO at highest FE ($mA/cm^2$) | Stability |
|---|---|---|---|---|---|
| NCNT-1[2] | 80% | CO | -0.78 V | 0.2 | 10 h |
| NCNT-2[3] | 80% | CO | -0.70 V | ~4.0 | N/A |
| Biomass[4] | 40% | CO | -0.82 V | 1.4 | ~5 h |
| g-$C_3N_4$/MWCNTs-1[5] | 98% | CO | -1.23 V | 90 | N/A |
| g-$C_3N_4$/MWCNTs-2[6] | 60% | CO | -0.45 V | N/A | N/A |
| P-OLC (This study) | 81% | CO | -0.65 V | 4.9 | 27 h |

## References For Supplementary Information


1. Frisch, M. J. et al.; Gaussian; Gaussian, Inc.: Wallingford CT, 2009.
2. Wu, J., Yadav, R. M.; Liu, M.; Sharma, P. P.; Tiwary, C. S.; Ma, L.; Zou, X.; Zhou, X. D.; Yakobson, I. B.; Lou, J.; Ajayan, P. M. *ACS Nano*, 2015, **9**, 5364-5371.
3. Sharma, P. P.; Wu, J.; Yadav, R. M.; Liu, M.; Wright, C. J.; Tiwary, C. S.; Yakobson, B. I.; Lou, J.; Ajayan P. M.; Zhou, X. D. *Angew. Chem. Int. Ed.*, 2015, **54**, 13701-13705.
4. Song, Y.; Chen, W.; Zhao, C.; Li, S.; Wei, W.; Sun, Y. Angew. Chem., Int. Ed., 2017, 36, 10980–10984.
5. Lu, X.; Tan, T. H.; Ng, Y. H.; Amal, R. *Chem.- Eur. J.*, 2016, **22**, 11991-11996.
6. Wang, H.; Jia, J.; Song, P.; Wang, Q.; Li, D.; Min, S.; Qian, C.; Wang, L.; Li, Y. F.; Ma, C.; Wu, T.; Yuan, J.; Antonietti, M.; Ozin, G. A. *Angew. Chem. Int. Ed.*, 2017, **56**, 7847-7852.